Estimation of Rail Wear Limits Based on Rail Strength Investigations

US Department
of Transportation

**Federal Railroad
Administration**

Office of Research and
Development
Washington, DC 20590

D.Y. Jeong
Y.H. Tang
O. Orringer

U.S. Department of Transportation
Research and Special Programs Administration
Volpe National Transportation Systems Center
Cambridge, Massachusetts 02142

DOT/FRA/ORD-98/07
DOT-VNTSC-FRA-98-13

December 1998
Final Report

REPORT DOCUMENTATION PAGE

Form Approved
OMB No. 0704-0188

1. AGENCY USE ONLY (Leave blank)	2. REPORT DATE	3. REPORT TYPE & DATES COVERED
	December 1998	Final Report - January 1997

4. TITLE AND SUBTITLE
Estimation of Rail Wear Limits Based on Rail Strength Investigations

5. FUNDING NUMBERS
R9002/RR928

6. AUTHOR(S)
David Y. Jeong,[1] Yim H. Tang,[1] and O. Orringer [1,2]

7. PERFORMING ORGANIZATION NAME(S) AND ADDRESS(ES)
[1] U.S. Department of Transportation
Research and Special Programs Administration
Volpe National Transportation Systems Center
Cambridge, MA 02142-1093
[2] Tufts University
Mechanical Engineering Department
Medford, MA 02155

8. PERFORMING ORGANIZATION REPORT
DOT-VNTSC-FRA-98-13

9. SPONSORING/MONITORING AGENCY NAME(S) AND ADDRESS(ES)
U.S. Department of Transportation
Federal Railroad Administration
Office of Research and Development
Washington, DC 20590

10. SPONSORING OR MONITORING AGENCY REPORT NUMBER
DOT/FRA/ORD-98/07

11. SUPPLEMENTARY NOTES

12a. DISTRIBUTION/AVAILABILITY
This document is available to the public through the National Technical Information Service, Springfield, VA 22161. This document is also available on the FRA web site at www. Fra.dot.gov.

12b. DISTRIBUTION CODE

13. ABSTRACT (Maximum 200 words)
This report describes analyses performed to estimate limits on rail wear based on strength investigations. Two different failure modes are considered in this report: (1) permanent plastic bending, and (2) rail fracture. Rail bending stresses are calculated using the classical theory of beams on elastic foundation. The effect of wear is modeled as a geometric change of the rail section due to loss of material from wear. Two different wear patterns are examined: (1) vertical rail-head height loss, and (2) gage-face wear from the side of the rail (referred to as gage-face side wear). An elementary plastic-collapse criterion is used to estimate wear limits based on failure by means of rail bending. An approximate method that was previously developed to analyze the growth of internal transverse defects is also applied to estimate wear limits on the basis of fracture strength. These analyses reveal that rail-wear limits estimated with the fracture-mechanics approach are more restrictive (i.e., conservative) than those based on the plastic-bending approach. Therefore, for safe operations on railroad tracks, allowable rail-wear limits should be estimated on the basis of fracture strength.

14. SUBJECT TERMS
detail fracture, dynamic load factor, fracture mechanics, fracture strength, gage-face wear, head-height loss, plastic collapse, yield strength, wear

15. NUMBER OF PAGES
44

16. PRICE CODE

17. SECURITY CLASSIFICATION OF REPORT	18. SECURITY CLASSIFICATION OF THIS PAGE	19. SECURITY CLASSIFICATION OF ABSTRACT	20. LIMITATION OF ABSTRACT
Unclassified	Unclassified	Unclassified	

PREFACE

In support of the Federal Railroad Administration's (FRA) Track Safety Research Program, the John A. Volpe National Transportation Systems Center (Volpe Center) has been conducting and managing research to develop technical information that can be used to support rational criteria for the preservation of safe operations on railroad tracks.

The Federal Railroad Administration (FRA) convenes biannual meetings of the Technical Resolution Committee (TRC) to address issues involving the application of FRA safety regulations. The mission of the TRC is to achieve consensus on the interpretation of existing regulations. The TRC charter allows for some discussion on whether safety standards should be revised, but such topics must be referred to the Rail Safety Advisory Committee (RSAC) for action. The RSAC was formed to facilitate negotiated rule-making for the purpose of revising the FRA safety standards.

One area of interest to the RSAC is the effect of rail-head wear on rail strength and structural integrity. The purpose of this report is to provide technical information regarding rail-wear limits developed on the basis of engineering analyses.

The analyses described in this report consider rail strength as either resistance to permanent plastic bending or resistance to fracture. The results from these analyses show that estimates for rail-wear limits based on the fracture mechanics approach are more restrictive (i.e., more conservative) than those based on permanent plastic bending. Therefore, for safe operations on railroad tracks, allowable rail-wear limits should be estimated on the basis of fracture strength.

METRIC/ENGLISH CONVERSION FACTORS

ENGLISH TO METRIC	METRIC TO ENGLISH
LENGTH (APPROXIMATE)	**LENGTH (APPROXIMATE)**
1 inch (in) = 2.5 centimeters (cm)	1 millimeter (mm) = 0.04 inch (in)
1 foot (ft) = 30 centimeters (cm)	1 centimeter (cm) = 0.4 inch (in)
1 yard (yd) = 0.9 meter (m)	1 meter (m) = 3.3 feet (ft)
1 mile (mi) = 1.6 kilometers (km)	1 meter (m) = 1.1 yards (yd)
	1 kilometer (km) = 0.6 mile (mi)
AREA (APPROXIMATE)	**AREA (APPROXIMATE)**
1 square inch (sq in, in^2) = 6.5 square centimeters (cm^2)	1 square centimeter (cm^2) = 0.16 square inch (sq in, in^2)
1 square foot (sq ft, ft^2) = 0.09 square meter (m^2)	1 square meter (m^2) = 1.2 square yards (sq yd, yd^2)
1 square yard (sq yd, yd^2) = 0.8 square meter (m^2)	1 square kilometer (km^2) = 0.4 square mile (sq mi, mi^2)
1 square mile (sq mi, mi^2) = 2.6 square kilometers (km^2)	10,000 square meters (m^2) = 1 hectare (ha) = 2.5 acres
1 acre = 0.4 hectare (he) = 4,000 square meters (m^2)	
MASS - WEIGHT (APPROXIMATE)	**MASS - WEIGHT (APPROXIMATE)**
1 ounce (oz) = 28 grams (gm)	1 gram (gm) = 0.036 ounce (oz)
1 pound (lb) = 0.45 kilogram (kg)	1 kilogram (kg) = 2.2 pounds (lb)
1 short ton = 2,000 pounds (lb) = 0.9 tonne (t)	1 tonne (t) = 1,000 kilograms (kg)
	= 1.1 short tons
VOLUME (APPROXIMATE)	**VOLUME (APPROXIMATE)**
1 teaspoon (tsp) = 5 milliliters (ml)	1 milliliter (ml) = 0.03 fluid ounce (fl oz)
1 tablespoon (tbsp) = 15 milliliters (ml)	1 liter (l) = 2.1 pints (pt)
1 fluid ounce (fl oz) = 30 milliliters (ml)	1 liter (l) = 1.06 quarts (qt)
1 cup (c) = 0.24 liter (l)	1 liter (l) = 0.26 gallon (gal)
1 pint (pt) = 0.47 liter (l)	
1 quart (qt) = 0.96 liter (l)	
1 gallon (gal) = 3.8 liters (l)	
1 cubic foot (cu ft, ft^3) = 0.03 cubic meter (m^3)	1 cubic meter (m^3) = 36 cubic feet (cu ft, ft^3)
1 cubic yard (cu yd, yd^3) = 0.76 cubic meter (m^3)	1 cubic meter (m^3) = 1.3 cubic yards (cu yd, yd^3)
TEMPERATURE (EXACT)	**TEMPERATURE (EXACT)**
[(x-32)(5/9)] °F = y °C	[(9/5) y + 32] °C = x °F

QUICK INCH - CENTIMETER LENGTH CONVERSION

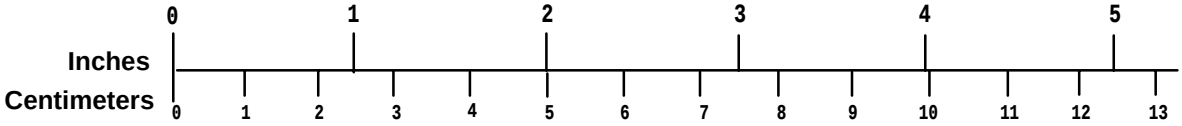

QUICK FAHRENHEIT - CELSIUS TEMPERATURE CONVERSION

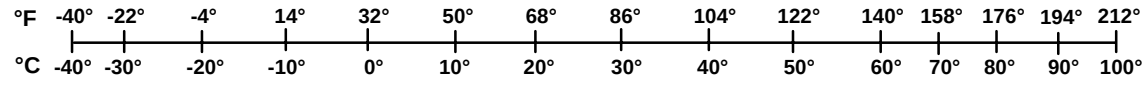

For more exact and or other conversion factors, see NIST Miscellaneous Publication 286, Units of Weights and Measures. Price $2.50 SD Catalog No. C13 10286

Updated 6/17/98

TABLE OF CONTENTS

LIST OF FIGURES

LIST OF TABLES

EXECUTIVE SUMMARY

In its April 1996 meeting, the FRA Technical Resolution Committee (TRC) discussed the question of how track inspectors should deal with heavily worn rail. Although the Track Safety Standards do not address rail wear, the TRC requested that technical information be developed on quantitative estimation of wear limits based on rail strength. The Volpe Center was asked to perform this task, and to do so has used an approximate method that was previously developed in support of the FRA Track Safety Research Program to determine rail section properties needed for rail stress analysis. The corresponding wear limits are based on strength criteria that consider failure as either permanent plastic bending or rail fracture. Rail-wear limits based on fracture strength assume the presence of an internal transverse defect known as the detail fracture. The study results show that the defect-based limits are more restrictive than those based on plastic bending. In other words, the fracture mechanics approach gives more conservative wear-limit estimates than the analysis based on permanent plastic bending. Therefore, for safe operations on railroad tracks, allowable rail-wear limits should be estimated on the basis of fracture strength. For all but the lightest rail sections considered, the limits for allowable wear were estimated as 0.5 inch head-height loss or 0.6 inch gage-face loss, under the assumption that the rail is inspected for internal defects every 20 million gross tons (MGT).

1. INTRODUCTION

Rail-wear limits have traditionally been based on strength to ensure that the rail can adequately support revenue service traffic without failure. In this report, wear limits are estimated from strength analyses that consider two failure modes: (1) permanent plastic bending, and (2) rail fracture from the presence of an internal transverse defect known as the detail fracture.[1] The mechanical properties of rail steel required in these analyses are yield strength and fracture toughness.

In the analyses described in this report, the rail is assumed to behave as a beam supported by a linear elastic foundation [1]. The longitudinal rail-bending stress is calculated from the application of a single vertical wheel load. In the strength analysis, the critical-load estimate is based on a plastic-collapse model in which attainment of yielding through the full depth of the rail is assumed. In the fracture strength analysis, the stress intensity factor for a detail fracture is equated to the nominal value of fracture toughness for rail steel. "Worst-case" vertical wheel loads are assumed in the determination of wear limits based on plastic-bending strength. Here, the worst-case load is defined as the wheel load expected to occur no more than once per 10^5 to 10^6 wheel passages. This critical or "worst-case" load is estimated from a correlation between actual freight-traffic load data and the AREA-recommended formula for dynamic load magnification factor. Lower loads corresponding roughly to the maximum expected once per train passage (or once per 400 wheel passages), are used to estimate the effects of rail wear on critical detail fracture (DF) size for rail failure by fracture. Rail-section properties needed in the beam-theory stress analysis are calculated using a methodology that assumes wear to occur from loss of material. Two wear patterns are considered: uniform loss of material from either the top of rail (referred to as vertical head-height loss) or the gage side of the rail (called gage-face side wear).

Vertical head-height loss occurs in virtually all track, and is the predominant mode of wear in tangent and shallow curves. Wear on the gage face of the rail is caused by contact loads applied to the side of the rail head by wheel flanges, and is most pronounced on curves greater than 3 to 4 degrees.

In this report, rail-wear limits are estimated for FRA track classes 2 through 5. Seven particular rail sections are considered: 70 ASCE, 85 ASCE, 100 RE, 115 RE, 132 RE, 136 RE, and 140 RE. Sections 2 and 3 describe the yield strength and fracture strength analyses, respectively, for worn rail. The estimation of worst-case wheel loads is described in Section 4. The results from these analyses are presented in Section 5. A discussion of the results and conclusions from the rail strength investigations are given in Section 6.

[1] Detail fractures are the most common transverse rail defect found in continuous welded rail (CWR).

2. STRENGTH ANALYSIS FOR WORN RAIL

Rail-wear limits can be estimated on the basis of yield or ultimate strength when longitudinal rail bending stresses are calculated. In the case of wear in terms of head-height loss, only the vertical component of the longitudinal bending stress is considered. Since gage-face wear occurs from lateral wheel-rail contact loads, the lateral load component of the longitudinal bending stress is considered in this wear case in addition to the vertical component.

A methodology was developed in Reference [2] to estimate section properties for worn rail. In this methodology, the actual rail cross-section is approximated by an idealized section consisting of three rectangular areas representing the head, web, and base of the rail (Figure 1). Rail-head wear is assumed to occur by a uniform loss of material from either the top of the head (referred to as vertical head-height loss) or the gage-side face (referred to as gage-face side wear). These two different wear patterns are illustrated in Figure 2 for an idealized rail section. Therefore, the physical loss of material from wear translates to a geometric change in the rail cross-section in the engineering analyses. In other words, rail strength is influenced by wear through changes in rail section properties due to wear. Various section properties for new or unworn rail are listed in Appendix A. The specific equations used to determine section properties for worn rail are given in Appendix B.

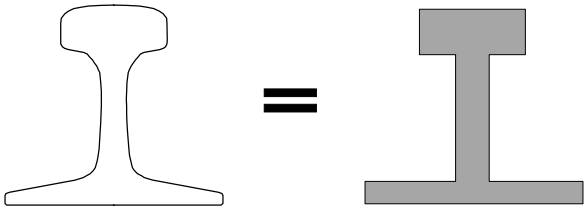

Figure 1. Actual and Idealized Rail Cross-Sections

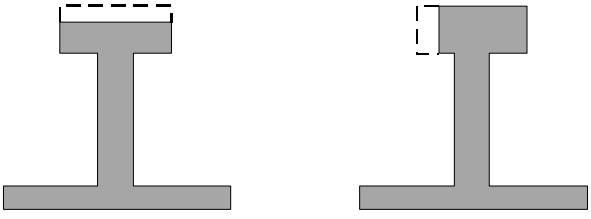

(a) Vertical head-height loss ***(b) Gage-face side wear***

Figure 2. Idealized Rail-Head Wear Patterns

2.1 Vertical Bending Component

For the present, it is convenient to assume that the entire rail cross-section remains elastic. Under this assumption, the longitudinal bending stress due to vertical rail bending is calculated from

$$\sigma_V(x) = \frac{M_V(x) \cdot c}{I_{yy}} \tag{1}$$

where $M_V(x)$ is the vertical bending moment as a function of longitudinal position along the rail, c is the distance from the centroid of the entire rail to the point of interest, and I_{yy} is the second area moment of inertia with respect to the horizontal axis through the rail centroid.

In the present study, bending stresses are calculated at the top of the rail; specifically, the upper gage corner of the rail head. Thus,

$$c = h - h_N \tag{2}$$

where h is the total rail height, and h_N is the distance from the bottom of the rail to the rail centroid. In addition, wear in terms of head-height loss is assumed to affect the rail strength through the geometric parameters in equation (1), namely, c and I_{yy}. Mathematically, these rail-section parameters are treated as functions of head-height loss or gage-face side wear.

The bending moment in equation (1) is calculated from beam-on-elastic-foundation theory [1], or

$$M_V(x) = -\frac{V}{4\lambda_V} e^{-\lambda x}(\cos\lambda_V x - \sin\lambda_V x) \tag{3}$$

where V is the vertical wheel load. It is evident from this equation that the maximum bending moment occurs directly beneath the wheel. Also, in this equation,

$$\lambda_V = \sqrt[4]{\frac{k_v}{4EI_{yy}}} \tag{4}$$

where E is the modulus of elasticity for rail steel (a value of 3×10^7 psi is assumed), and k_v is the vertical foundation stiffness (which is assumed to vary depending on FRA track classification).

2.2 Lateral Bending Component

Similar equations to those given for vertical bending can be written to determine the lateral component of the longitudinal rail-bending stress. The magnitude of the lateral bending component at the upper gage corner of the rail is given by

$$\sigma_L(x) = \frac{M_L(x) \cdot w_H}{2I_{zz}} \tag{5}$$

where I_{zz} is the second area moment of inertia with respect to the vertical axis through the rail centroid, and w_H is the width of the rail head. In addition, the lateral bending moment as a function of longitudinal position along the rail is

$$M_L(x) = -\frac{L}{4\lambda_L} e^{-\lambda_L x}(\cos\lambda_L x - \sin\lambda_L x) \tag{6}$$

where L is lateral wheel load and

$$\lambda_L = \sqrt[4]{\frac{0.85k_v}{4EI_{zz}}}\,. \tag{7}$$

In this equation, the lateral foundation stiffness is assumed to be 0.85 times the vertical foundation stiffness [4].

2.3 Strength-Based Wear-Limit Estimation

The rail bending equations presented in Sections 2.1 and 2.2 can be combined to derive expressions for maximum elastic load, V_e, under which the greatest stress magnitude reaches the material yield strength, $_{YLD}$. For vertical bending only (Section 2.1), combining equations (1) to (3) gives

$$V_e = \frac{\sigma_{YLD}}{(h - h_N)/4\lambda_V I_{yy}} \tag{8}$$

If lateral bending (Section 2.2) is included, a combined-stress expression from equations (1) to (3), (5), and (6) gives

$$V_e = \frac{\sigma_{YLD}}{\left[\frac{h - h_N}{4\lambda_V I_{yy}} + \left(\frac{w_H}{8\lambda_L I_{zz}}\right) \cdot \frac{L}{V}\right]} \tag{9}$$

where L/V is a specified ratio of lateral-to-vertical wheel load ratio. Comparison of equations (8) and (9) shows that V_e for the combined-loading case is always somewhat less than V_e for purely vertical bending. In the following development,

purely vertical bending will be assumed for the analysis of vertical head-height loss, but combined bending will be assumed for the analysis of gage-face side wear.

Maximum elastic load is a convenient quantity to calculate from beam theory, but is too low to be a realistic measure of rail strength. A better quantity for this purpose is the plastic-collapse load, V_o, under which a rail would be expected to form a large permanent kink. Plasticity theory can be applied to make estimates of V_o under certain simplifying assumptions.

For example, well established results presented by Hodge [3] give simple formulas for the maximum elastic and plastic collapse loads; in terms of vertical bending moments, M_e and M_o; for beams of rectangular cross-section, and thin, wide-flanged I-sections assumed to consist of elastic-perfectly-plastic material (Figure 3). The ratio of M_o/M_e is found to be 1.05 to 1.1 for I-sections of height and width comparable to rail sections. With such a ratio available, in principle, one may calculate V_e and estimate $V_o = (M_o/M_e)V_e$ because the proportionality between applied load and applied bending moment remains linear even as the beam yields.

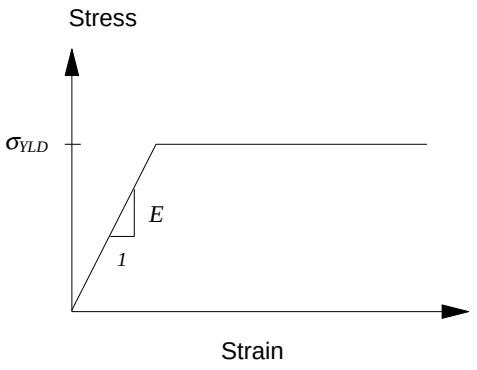

Figure 3. Stress-Strain Curve for Elastic-Perfectly-Plastic Material Behavior

The equivalent section models shown in Figure 2, and summarized in Appendix B, have been used to follow a similar procedure in the present case. Figure 4 is a schematic of the stress distributions for the maximum elastic moment, M_e, and the plastic collapse moment, M_o.[2] Strictly speaking, the estimates indicated in Figure 4 are valid only for symmetrical wear (head-height loss) and purely vertical bending. However, the ratio of M_o/M_e based on vertical bending has also been applied to the side-wear case, neglecting the small effects of lateral bending and the cross-product terms associated with asymmetrical side wear.

[2] In Figure 4, the location of the neutral axis for the elastic stress distribution coincides with the location of the rail centroid. For the fully-plastic case, however, the neutral axis shifts to a location that divides the rail cross-sectional area into two equal halves.

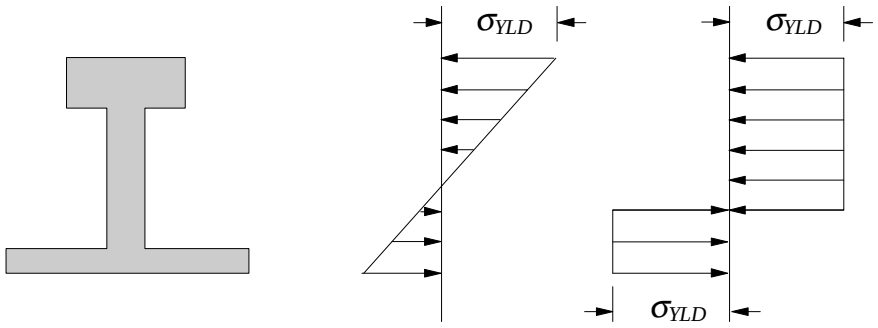

Figure 4. Elastic and Fully-Plastic Stress Distributions in an Idealized Rail Section

Ratios of M_o/M_e were found to range roughly from 1.4 to 1.6 for the case of vertical head-height loss, and from 1.4 to 2.0 for the case of gage-side wear. Tables 1 and 2 summarize these estimates for the two different wear patterns and the various rail sections considered in this report.

Table 1. M_o/M_e Ratios for Vertical Head-Height Loss

Wear (%HA)	*70 ASCE*	*85 ASCE*	*100 RE*	*115 RE*	*132 RE*	*136 RE*	*140 RE*
0	1.37	1.36	1.38	1.40	1.39	1.39	1.38
20	1.40	1.40	1.41	1.43	1.43	1.42	1.41
40	1.42	1.44	1.44	1.48	1.47	1.47	1.45
60	1.43	1.47	1.48	1.54	1.52	1.52	1.51
80	1.46	1.54	1.59	1.65	1.61	1.61	1.60

Table 2. M_o/M_e Ratios for Gage-Face Side Wear

Wear (%HA)	*70 ASCE*	*85 ASCE*	*100 RE*	*115 RE*	*132 RE*	*136 RE*	*140 RE*
0	1.37	1.36	1.38	1.40	1.39	1.39	1.38
20	1.46	1.46	1.46	1.49	1.48	1.48	1.47
40	1.54	1.56	1.56	1.60	1.58	1.59	1.58
60	1.63	1.68	1.67	1.74	1.72	1.73	1.72
80	1.79	1.88	1.91	1.99	1.94	1.95	1.97

Strength-based limits on rail wear are estimated as follows. Consider first the case of head-height loss, Δh, for which purely vertical bending is assumed in the analysis. With the rail section properties modified as described in Appendix B, calculations are made for the corresponding maximum elastic load V_e as a function of Δh from

equation (8), and the moment ratio M_o/M_e as outlined above. The rail collapse load is then estimated as

$$V_o = \frac{M_o}{M_e} \cdot V_e \tag{10}$$

As indicated in Figure 5, V_o decreases as the head-height loss, Δh, increases, and the wear limit is determined by the intersection of the V_o versus Δh curve with the worst-case load line, V_{max} (See Section 4 for V_{max}).

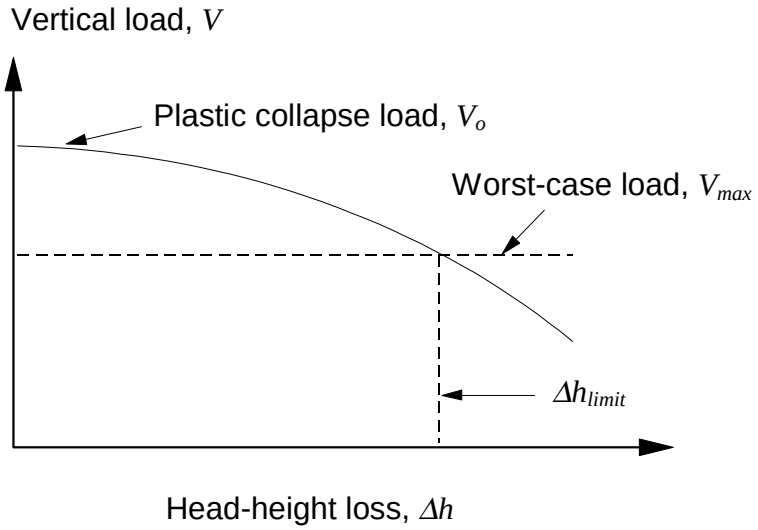

Figure 5. Schematic for Estimation of Head-Height Wear Limit

A similar procedure is followed to estimate the limit for gage-face side wear. In this case, equation (9) is used to calculate V_e with a lateral-to-vertical load ratio L/V = 0.2, assumed to represent average track curvatures of less than 3 degrees. The side-wear limit is then determined from a plot similar to the schematic in Figure 5.

3. FRACTURE MECHANICS ANALYSIS FOR WORN RAIL

It is also worthwhile to estimate how rail wear affects critical size for rail failure, on the basis of fracture strength. In this case, the rail is assumed to contain an internal transverse defect. Linear elastic fracture mechanics principles are applied to determine the amount of wear that would result in rail fracture when a rail containing a detail fracture (DF) of a given (assumed) size experiences a "once-per-train" wheel load. Wear is assumed to approach a limit when detail fractures can grow from a barely detectable size to a critical size in less than one-half an inspection period. The growth behavior of detail fractures in rails has been studied in previous research [4].

3.1 Stress Intensity Factor for Detail Fractures

For sizes smaller than 50% of the rail-head area (%HA), the detail fracture is assumed to be an embedded elliptical flaw located in the vicinity of the upper gage corner of the rail head (Figure 6). The dimensions of the defect are characterized by the semi-major and semi-minor axes of the ellipse, a and b, respectively. Examinations of rails containing detail fractures have revealed that the aspect ratio, b/a, is typically equal to 0.7. The center of the detail fracture is characterized by its location relative to the unworn running surface, z^*, and the vertical mid-plane, y.

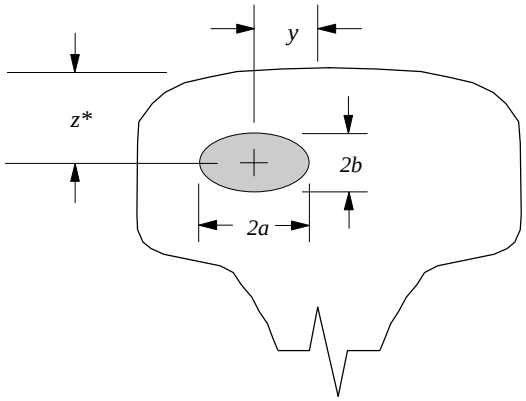

Figure 6. Schematic of a Detail Fracture in the Rail Head

A relationship between the location of the DF center and DF size in 136 RE rail sections was derived empirically in the previous study [4]

$$y = 1.1874 - 2.9523 \cdot \left(\frac{A}{A_H}\right) + 3.4306 \cdot \left(\frac{A}{A_H}\right)^2 \qquad (11)$$

$$z^* = 0.6213 + 1.7580 \cdot \left(\frac{A}{A_H}\right) - 1.7933 \cdot \left(\frac{A}{A_H}\right)^2 \tag{12}$$

where A is the size of the detail fracture in terms of area ($A = 0.7\pi a^2$), and A_H is the cross-sectional area of an unworn or new rail head. The parabolic trend characterized by these equations for 136 RE rail was assumed to be constant for other rail sizes. Also, the depth of the DF center below the rail running surface and inward from the gage face was assumed to be independent of rail size; i.e., varying only with the defect area ratio, A/A_H.

The stress intensity factor or "K" formula for the embedded elliptical flaw shown schematically in Figure 6 has the following mathematical form

$$K_I = \frac{2}{\pi} \cdot M_s\left(\frac{b}{a}\right) \cdot M_1(a) \cdot \sigma_\infty \cdot \sqrt{\pi a} \tag{13}$$

where σ_∞ is the longitudinal tensile stress at the defect center due to rail bending and other effects, a is the semi-major axis of the elliptical flaw, M_s is a magnification factor to account for the elliptical flaw shape, and M_1 is a magnification factor to account for finite boundaries. The magnification factors for detail fractures were derived in Reference [4]. For instance, for an elliptical flaw aspect ratio of b/a = 0.7, M_s = 0.984. The finite-section magnification factor was modified from the original formulation to account for loss of rail-head area because of wear, and is given by

$$M_1(a) = \sqrt{\frac{2}{\pi}\left(\frac{1-\frac{X}{100}}{\frac{0.7\pi a^2}{A_H}}\right)\tan\left[\frac{\pi}{2\left(1-\frac{X}{100}\right)}\cdot\left(\frac{0.7\pi a^2}{A_H}\right)\right]} \times$$

$$\left[\frac{0.63 + \frac{2.02}{\left(1-\frac{X}{100}\right)}\cdot\left(\frac{0.7\pi a^2}{A_H}\right) + 0.37\left[1-\sin\left[\frac{\pi}{2\left(1-\frac{X}{100}\right)}\cdot\left(\frac{0.7\pi a^2}{A_H}\right)\right]\right]^3}{\cos\left[\frac{\pi}{2\left(1-\frac{X}{100}\right)}\cdot\left(\frac{0.7\pi a^2}{A_H}\right)\right]}\right] \tag{14}$$

where X is a measure of wear in terms of percent rail-head area (%HA). The aspect ratio of 0.7 for typical detail fractures has been included in equation (14).

The K formula given in equation (13) applies to remote uniform tension only. Therefore, a stress-gradient magnification factor must also be applied to the K

formula if the rail head is subjected to a non-uniform stress field, which is the case when the rail is subjected to combined bending from both vertical and lateral loading. The stress-gradient or non-uniform stress magnification factor depends on the ratio of lateral to vertical wheel load as well as defect size relative to the unworn rail head area. The formalism to calculate the stress-gradient or non-uniform stress magnification factor is given in Appendix C. Appendix C also includes tabulated values of the stress-gradient magnification factors for a 132 RE rail section with various levels and types of wear, lateral-to-vertical load ratios, and DF sizes.

3.2 Stress Analysis for Rails with Detail Fractures

The magnitude of the stresses that drive the growth of detail fractures is assumed to be a linear superposition of residual, thermal, and bending stresses. Thus, the stress intensity factor formula for a detail fracture is given by

$$K_I = \frac{2}{\pi} \cdot M_s\left(\frac{b}{a}\right) \cdot M_1(a) \cdot \left[\sigma_R + \sigma_T + M_G(a) \cdot \sigma_B\right] \cdot \sqrt{\pi a} \tag{15}$$

where σ_R is the residual stress, σ_T is the thermal stress, M_G is the stress gradient or non-uniform stress magnification factor, and σ_B is the bending stress.

A relationship between the magnitude of tensile residual stress in the rail head and the DF size has been developed on the basis of experimental data obtained from two separate tests [4], [5] conducted at the Facility for Accelerated Service Testing (FAST)

$$\sigma_R = \begin{cases} 30 - 2.125 \cdot \left(\frac{A}{A_H} \times 100\right) & \text{for } \ 0\%HA \le \left(\frac{A}{A_H} \times 100\right) \le 10\%HA \\ 10 - 0.125 \cdot \left(\frac{A}{A_H} \times 100\right) & \text{for } \left(\frac{A}{A_H} \times 100\right) > 10\%HA \end{cases} \tag{16}$$

where $(A/A_H \times 100)$ represents the DF size in percentage of rail-head area (%HA).

Thermal stresses for fully restrained CWR in tangent track can be calculated from

$$\sigma_T = E\alpha\Delta T \tag{17}$$

where α is the linear coefficient of thermal expansion, E is the modulus of elasticity, and ΔT is the temperature difference between the in-service temperature and the neutral or stress-free temperature. In the present calculations, ΔT is an assumed variable.

Rail-bending stresses comprise both the vertical and lateral bending components, as described previously in Section 2 for the rail strength analysis. For a rail modeled as a beam on elastic foundation, the maximum tensile stress in the rail head occurs at some distance away from the point of load application. This phenomenon is referred to as "reverse" bending. In terms of absolute value, the maximum bending moment occurs directly beneath the wheel load. Referring to Figure 7, the location of the maximum "reverse" moment for vertical bending relative to the wheel position is defined by

$$x_0 = \frac{\pi}{2\lambda_V} \tag{18}$$

where λ_V is calculated from equation (4).

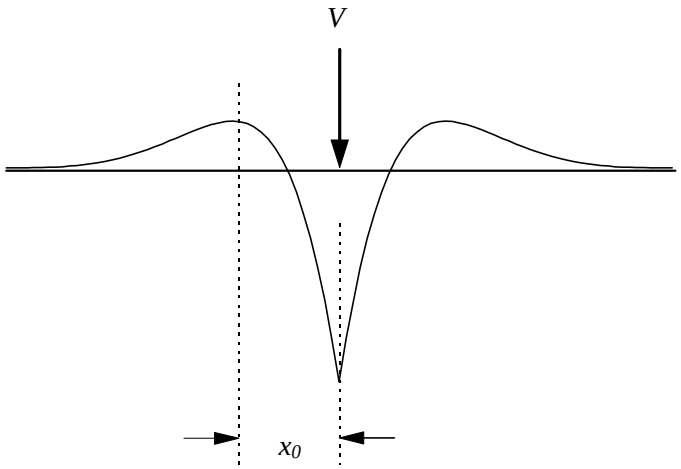

Figure 7. Bending Moment Distribution for a Single Wheel Load

Therefore, the bending stress used in equation (15) for the fracture analysis is calculated from

$$\sigma_B = \frac{M_V(x_0)\cdot(h - h_N)}{I_{yy}} + \frac{M_L(x_0)\cdot w_H}{2I_{zz}} \tag{19}$$

where the vertical and lateral bending moments are defined by equations (3) and (6), respectively.[3]

[3] The small effect of the cross-product terms associated with asymmetrical bending has been neglected in equation (19).

3.3 Fracture-Mechanics-Based Wear-Limit Estimation

Rail-wear limits based on the fracture mechanics approach are estimated by combining results from two separate sets of calculations. In the first set of calculations, rail wear is determined as a function of critical DF size. In other words, equation (15) is set equal to the fracture toughness of rail steel for different critical DF sizes and different levels of rail wear. Results from this numerical procedure are shown schematically in Figure 8. In the present analysis, the fracture toughness for rail steel, K_{IC}, is assumed to be 35 ksi-in$^{1/2}$. Also, an extreme temperature difference from the neutral or stress-free temperature of 50°F is assumed. In addition, a dynamic magnification is applied to magnify the magnitude of a static wheel load during calculation of the stress intensity factor. Details of the dynamic wheel load calculation for this purpose (referred to as the 0.8-σ load level) are described in Section 4.

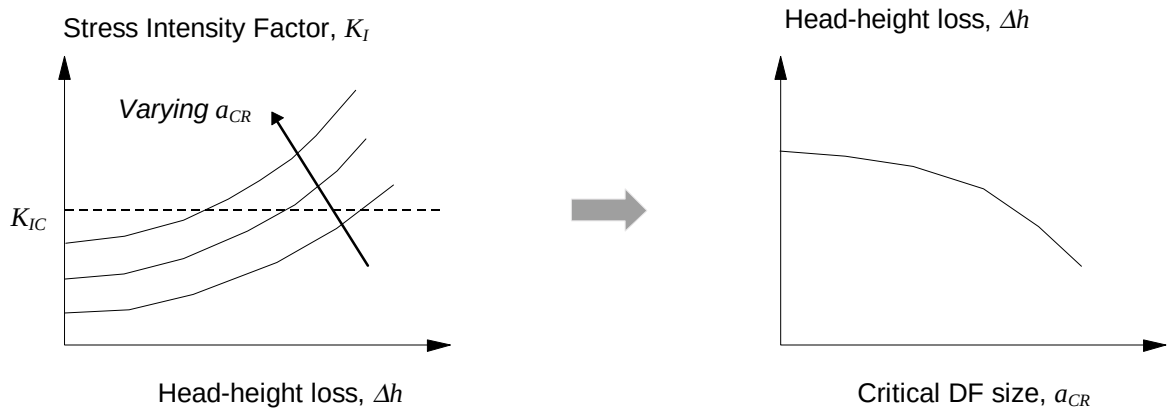

Figure 8. Schematic for Estimating Rail Wear as a Function of Critical DF Size

When we consider only the results from this first set of calculations, the question is: what critical-size defect should be considered in estimating the rail-wear limit? To answer this question, we assume that rail wear becomes critical (i.e., reaches a limit) when detail fractures can grow from a barely detectable size (assumed to be 5% HA) to a critical size in less than one typical inspection interval. For this purpose, we assumed 20 MGT. Thus, a second set of calculations is performed to determine the DF size that will be reached after 20-MGT traffic accumulation for various levels of rail wear, assuming an initial DF size of 5% HA. In these DF-growth calculations, a moderate temperature differential of 15°F is assumed. Figure 9 shows a schematic of the results from this second set of calculations. Reference [4] describes propagation analyses of detail fractures, which are used in the present calculations.

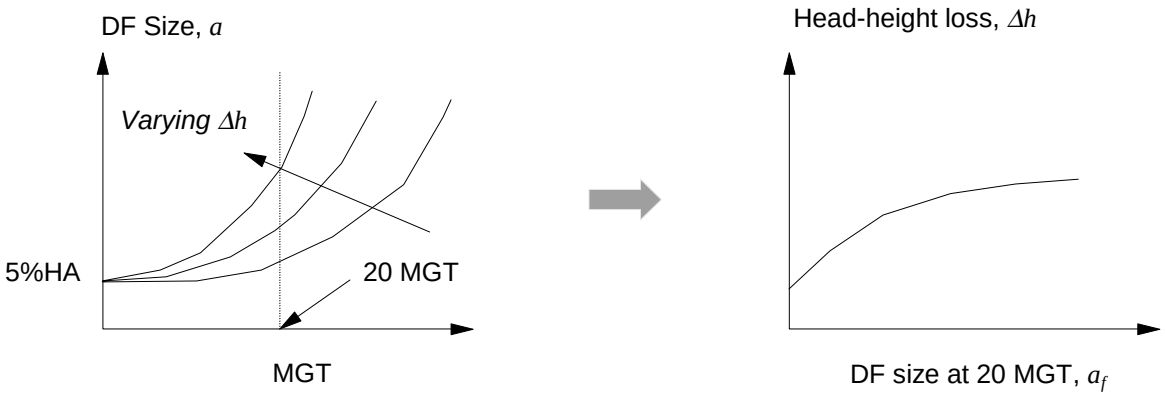

Figure 9. Schematic for Estimating Rail Wear as a Function of DF Size after 20 MGT from Initial Size of 5% HA

The results from the two sets of calculations described above can be combined, as shown in the schematic diagram in Figure 10. The intersection of the two curves; one based on fracture toughness and the other based on DF-growth rate, defines the limit for rail wear. Although the schematic diagrams shown in Figures 8 through 10 consider rail wear as head-height loss, the numerical procedures described in this section are also applicable for the case of gage-side wear.

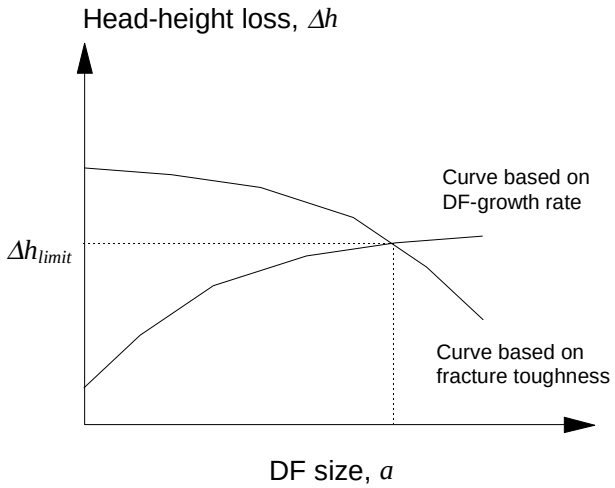

Figure 10. Estimate of Rail-Wear Limit Based on Fracture Strength

4. WORST-CASE LOAD ESTIMATION

Car body and truck dynamic motions (pitch, bounce, and rocking) cause wheel loads to vary at frequencies up to 10 Hz. For a given static wheel load, V, this dynamic load $V \pm V_D$ can be modeled as a Gaussian random process with probability density functions:

$$p(V \pm V_D) = \frac{1}{c_v V \sqrt{2\pi}} \exp\left[-\frac{(\pm V_D)^2}{2(c_v V)^2} \right] \tag{20}$$

where the coefficient of variation, c_v, scales the root-mean-square dynamic increment in terms of the static load. In measurements of actual data, however, differences have been observed between dynamic load increments and decrements. The statistical variation of dynamic loads should then be modeled with two one-sided Gaussian distributions to account for these observed differences.[4] A schematic of these distribution functions is shown in Figure 11. The coefficient of variation corresponding to the dynamic load increment, c_v^+, is applicable in determining the worst-case load.

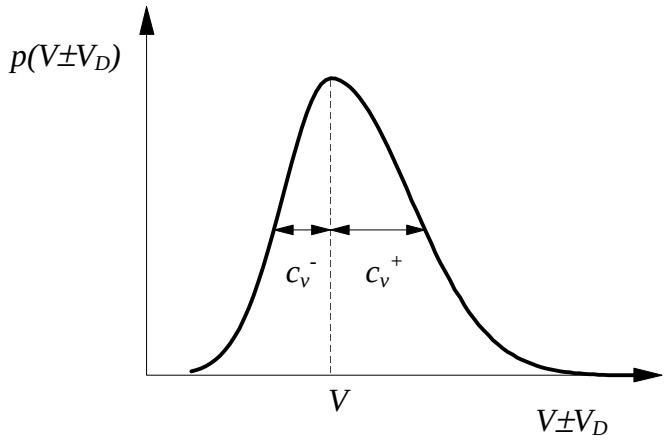

Figure 11. Schematic of a Two-Sided Gaussian Distribution Function

Physically, the worst-case load may be caused by a combination of several factors that include: (1) track irregularities and irregular track stiffness due to variable characteristics and settlement of the ballast; (2) discontinuities at welds, joints, and switches; (3) irregular rail-running surface (e.g., corrugated rail); (4) defects in vehicles such as wheel flats and wheel eccentricity; and (5) vehicle dynamics such as natural vibrations and hunting. Mathematically, the worst-case load is the average static wheel load multiplied by an extreme dynamic load magnification

[4] In addition, separate distributions are usually required to match the dynamic behavior of lightly and heavily loaded cars. To simplify the present analysis, however, fully loaded cars are considered.

factor. The dynamic effect is assumed to increase with train speed, and its mathematical relationship to the coefficient of variation is discussed in the following text.

Procedures are described in Orringer, et al., [4] to determine the coefficients of variation from load data given in the form of either exceedance curves or cumulative probability curves. Results from applying these procedures to freight-traffic load data from various sources are listed in Table 3. Table 3 is an abstract, from Orringer, et al., [4] of those results for which c_v^+ values can be related to loaded freight train speeds.

Table 3. Coefficients of Variation for Dynamic Vertical Load

	Environment Description [Ref.]	***Average Wheel Load (kips)***	***Speed (mph)***	c_v ***for*** $+V_D$
1	FAST, concrete tie, 1977 [7].	30.5	40 to 45	0.26
2	Loaded coal hopper car over 1,900 miles on six midwestern and eastern railroads [8].	30.0	15 to 30 30 to 45 45 to 60	0.20 0.17 0.22
3	DOT-112A, 33,000-gal tank car over 114 miles of a midwestern railroad mainline [8].	30.0	15 to 30 30 to 45 45 to 60	0.17 0.25 0.60
4	Hopper car loaded with crushed rock over 182 miles on a western railroad mainline [8].	30.0	15 to 30 30 to 45 45 to 60 > 60	0.08 0.10 0.11 0.12
5	FAST, concrete tie, circa 1977 [9].	27.7	40 to 45	0.30
6	Northeast Corridor, freight, concrete tie, Edgewood, MD, 1984 [10].	24.17 24.32	45 to 70	0.31 0.33

In the present analysis, the “worst-case” load can be defined in terms of the number of standard deviations above the mean value. The coefficient of variation, c_v, is related to the standard deviation by the static wheel load, V, as given in the following expression

$$c_v = \frac{\sigma}{V} \tag{21}$$

As indicated in Table 3, the coefficient of variation appears to vary with speed. This is consistent with the American Railroad Engineering Association (AREA) formula for dynamic load factor [6]

$$DLF = 1 + \frac{33v}{100D} \tag{22}$$

where v is the train speed (in miles per hour) and D is the wheel diameter (in inches).

For the purpose of load estimation, c_v can be considered as comparable to the term $33v/100D$ in the AREA formula. Figure 12 compares this term with the c_v data from Table 3. With only one exception, the formula term bounds the data in Table 3, and is therefore a reasonable representation of the service environment.

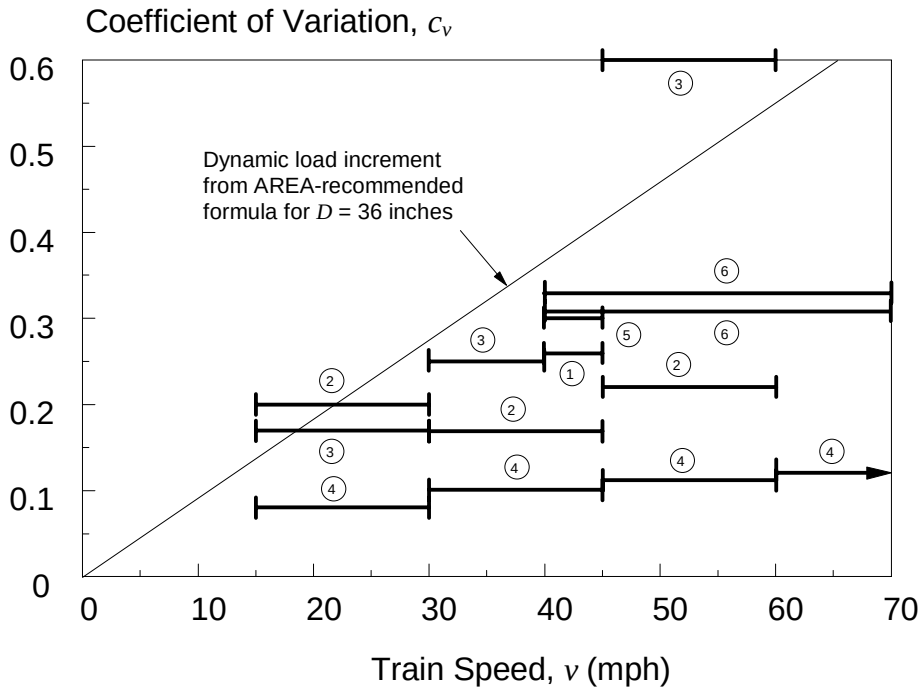

Figure 12. Speed Dependence on Coefficient of Variation and Dynamic Load Increment

Figure 13, reproduced from Orringer, et al., [4] shows the numbers of extreme-valued peak dynamic wheel loads measured in a field test on the Northeast Corridor in the early 1980s [10]. Table 4 summarizes the results for freight trains, which were typically operated at 60 mph through the instrumented site. Taking v = 60 mph and assuming that the extreme loads came from loaded 100-ton cars (corresponding to a static load, V, equal to 33 kips, and a wheel diameter, D, equal to 36 inches), we may apply the previous analysis to estimate the standard deviation as $\sigma = c_v V = 18.2$ kips. Thus, the range of 55 to 80 kips for extreme loads listed in Table 4 can be interpreted as roughly 1.2-σ to 2.6-σ events.

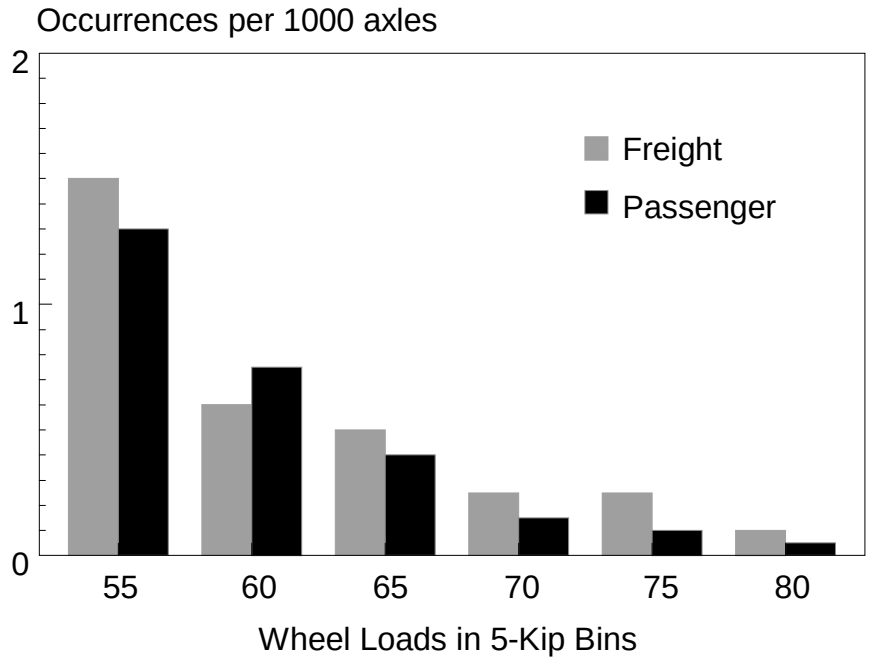

Figure 13. Histogram of Extreme Wheel Loads Measured on the Northeast Corridor

Table 4. Summary of Freight-Car Wheel-Load Histogram

Peak Load V_{peak} ***(kips)***	***Occurrences per 1000 Axles, n***
55	1.50
60	0.60
66	0.50
70	0.25
75	0.25
80	0.10

Although the peak values in Table 4 occur infrequently, they cannot be assumed to bound the worst case because the loads were measured only for a limited time at a single site. Therefore, it is necessary to extrapolate from the available data to estimate worst-case loads for various operating speeds. For this purpose, the regression formula

$$V_{peak} = \frac{2.4 - \log_{10} n}{0.042} \tag{23}$$

has been derived from a least-square-error analysis of the data listed in Table 4. Figure 14 compares equation (23) with the data points.

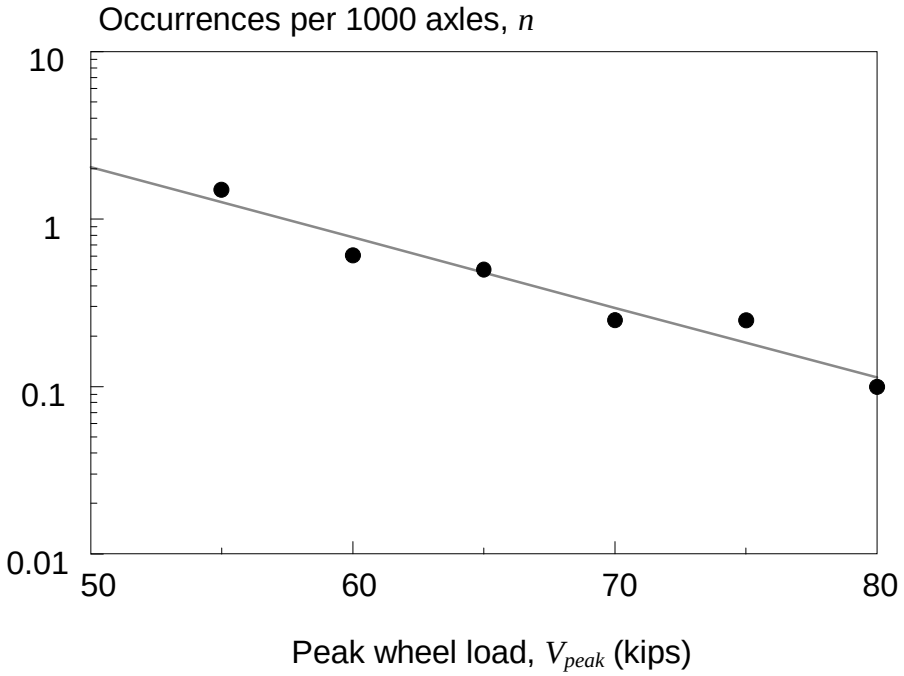

Figure 14. Regression for Occurrence Rate versus Peak Load

For randomly occurring events such as peak loads, the generally accepted definition of a worst-case event for the purpose of risk analysis is one expected to be exceeded no more often than once in 10^5 to 10^6 times.[5] For example, when the Gaussian distribution is used to model a random process, the 5-σ level is sometimes used to define the worst case. The 5-σ level of a Gaussian process has an exceedance rate of 1.6×10^{-6}, which lies within the range mentioned above. There is no justification for applying the Gaussian model to extreme wheel loads, but it is reasonable to adopt the 1.6×10^{-6} exceedance rate per axle passage as a worst-case criterion. Also, since there is no significant numerical difference between exceedance and occurrence rates at these extremes, we may take the corresponding occurrence rate as $n = 1.6 \times 10^{-3}$ per thousand axles and apply equation (23) to estimate the worst-case load as

$$V_{\max} = \frac{2.4 - \log_{10}(1.6 \times 10^{-3})}{0.042} \cong 124 \text{ kips} \qquad (24)$$

[5] For example, the current U.S. Army fatigue-life specification for new rotorcraft is based on the so-called “six-nines” reliability, or probability of failure of one in a million [11].

The above worst-case load estimate applies to the Northeast Corridor field-test site, for which σ = 18.2 kips was derived earlier as the standard deviation of the entire dynamic load range. Thus, the 5-σ dynamic load increment above the static wheel load appears to be a reasonable criterion for estimating worst-case wheel loads at operating speeds and/or wheel diameters other than those associated with the test site. Table 5 summarizes the worst-case loads estimated for the maximum operating speeds allowed on track classes 2 through 5, assuming a 33-kip static load and a 36-inch wheel diameter. The right-hand column lists suggestions for typical and minimum rail sections representative of track construction for the corresponding class. In the wear-limit analyses, vertical foundation stiffness is assumed to vary with different track classifications. The assumed values for vertical foundation stiffness for each track class are also listed in Table 5.

The load level selected as a basis for wear-limit estimation depends on the mode of failure assumed. For a strength-based limit, the wear process reduces plastic bending strength more or less uniformly along many rail lengths. Therefore, one must expect the reduced strength at a point where the worst possible combination of track irregularity and vehicle dynamics may occur, and it follows that the 5-σ load level is an appropriate basis. For a fracture-strength-based limit, however, the assumed mode of failure is propagation of a fatigue crack to fracture. To realistically treat this case requires one to recognize that sparsely distributed cracks (typically, 0.25 to 2 per track mile) are not necessarily found where the worst dynamic loads occur. A realistic extreme load basis for this case is the level expected once per train passage; i.e., about once per 400 axles, assuming a 100-car freight train. The corresponding value of n in equation (23) would be 2.5 per 1000 axles, which gives a value of V_{max} equal to 47.7 kips, corresponding to a 0.8-σ load level (assuming a 33-kip static wheel load). Table 5 also lists values of worst-case loads based upon the 0.8-σ load level, which are subsequently applied in the fracture mechanics calculations for estimating rail-wear limits.

Table 5. Representative Worst-Case Load Estimates with Corresponding Foundation Stiffness and Rail Sections

FRA Track Class	*Max. Train Speed v (mph)* [(a)]	*Coefficient of Variation c_v* [(b)]	*Standard Deviation σ (kips)* [(c)]	*Worst-Case Load V_{max} (kips)* [(d)]	*Vertical Foundation Stiffness k_v (psi)*	*Rail Section*
2	25	0.23	7.6	39/71	1,000	70 ASCE 85 ASCE 100 RE 115 RE
3	40	0.37	12.1	43/94	2,000	85 ASCE 100 RE 115 RE 132 RE
4	60	0.55	18.2	48/124	2,000	115 RE 132 RE 136 RE 140 RE
5	80	0.73	24.1	52/154	5,000	115 RE 132 RE 136 RE 140 RE

NOTES:

(a) Maximum train speeds are based on FRA Track Safety Standard 213.9 for freight traffic.

(b) Coefficient of variation calculated from: $c_v = 33v/100D$, where D = 36 inches.

(c) Standard deviation calculated from: $\sigma = c_v V$, where V = 33 kips.

(d) Worst-case loads are calculated from: $V_{max} = V + 0.8\sigma$ and $V_{max} = V + 5.0\sigma$. The loads corresponding to 0.8-σ above the static value were applied to the fracture mechanics analysis, and those for 5-σ were used in the estimates based on permanent bending strength.

5. RESULTS

Figure 15 shows rail-wear estimates of vertical head-height loss based on rail strength. Four different rail sizes are considered for each track class. As the track class increases from Class 2 to Class 4 (implying increased maximum train speed, higher worst-case loads, and improved foundation stiffness), the wear limit for a given rail section decreases. The estimated wear limits for Class 4 and 5 are practically equal. In these results, the yield strength for rail steel was assumed to be 90 ksi.

Rail-wear limits for side wear estimated on the basis of rail strength are shown in Figure 16. As in the case for vertical head-height loss, limits on side wear for both Class 4 and Class 5 track are effectively the same.

Rail-wear limits for head-height loss based on the fracture mechanics analyses are shown in Figure 17. In these analyses, the fracture toughness of rail steel has been assumed to be 35 ksi-in$^{1/2}$. The wear-limit estimates based on the fracture-strength approach are roughly 30 to 40% less than those based on the elastic-plastic bending analysis. Similarly, results for the side-wear limit are shown in Figure 18. Again, the wear-limit estimates based on the fracture analysis are about one-third of those based on permanent rail bending.

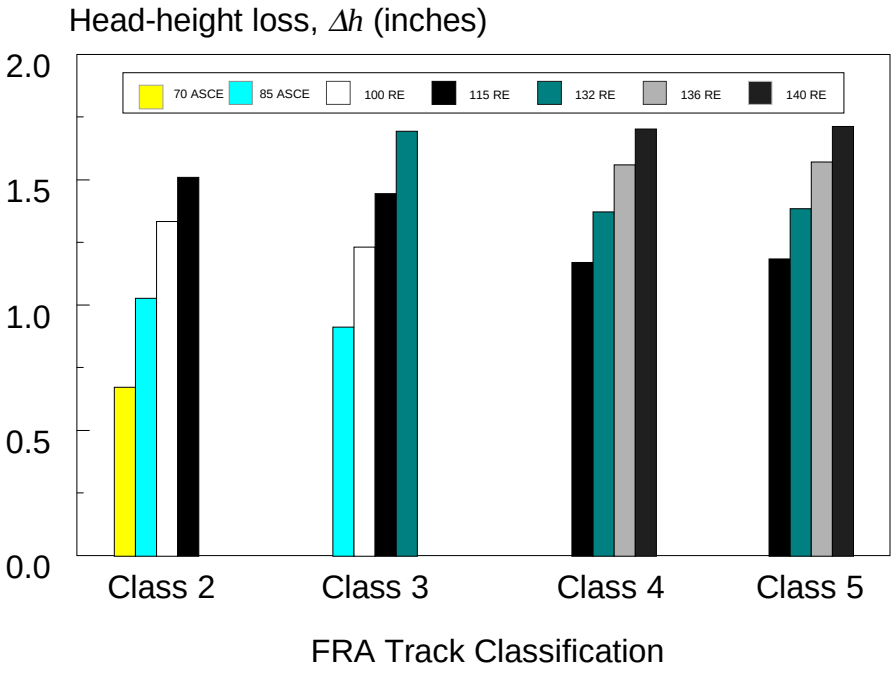

Figure 15. Wear-Limit Estimates for Head-Height Loss Based on Rail Strength

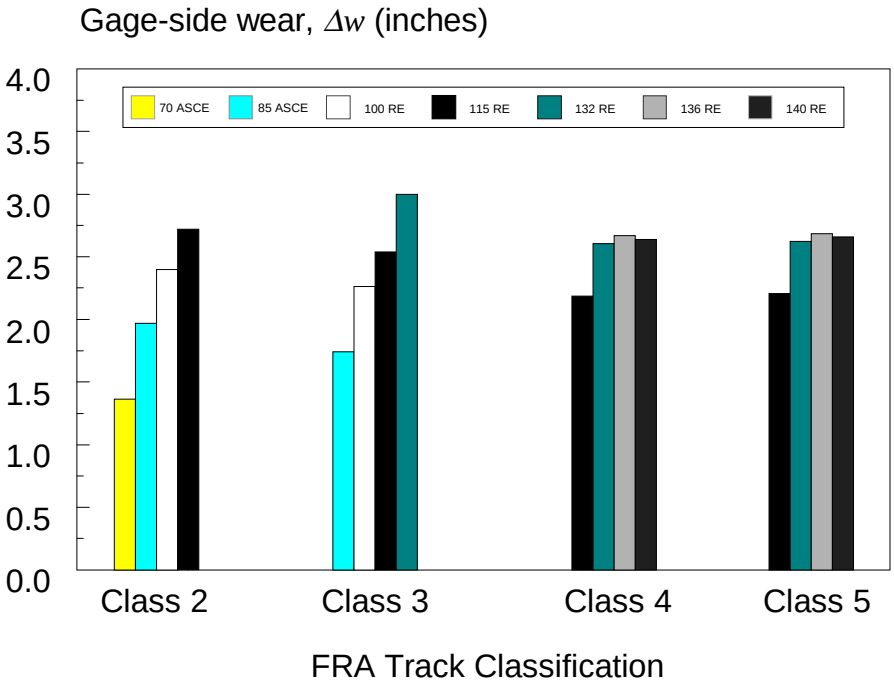

Figure 16. Wear-Limit Estimates for Side Wear Based on Rail Strength

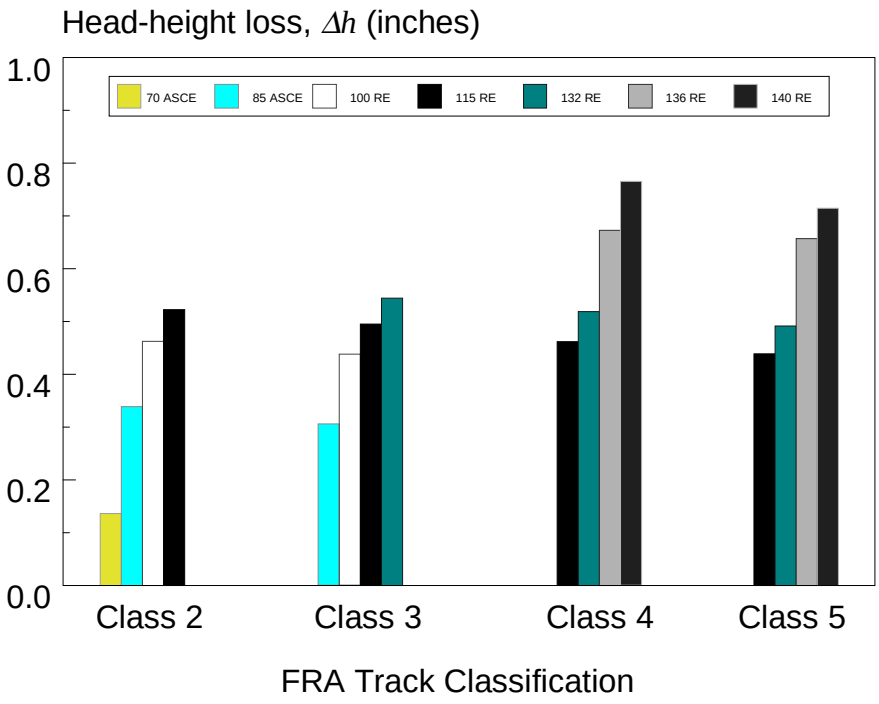

Figure 17. Wear-Limit Estimates for Head-Height Loss Based on Fracture Strength

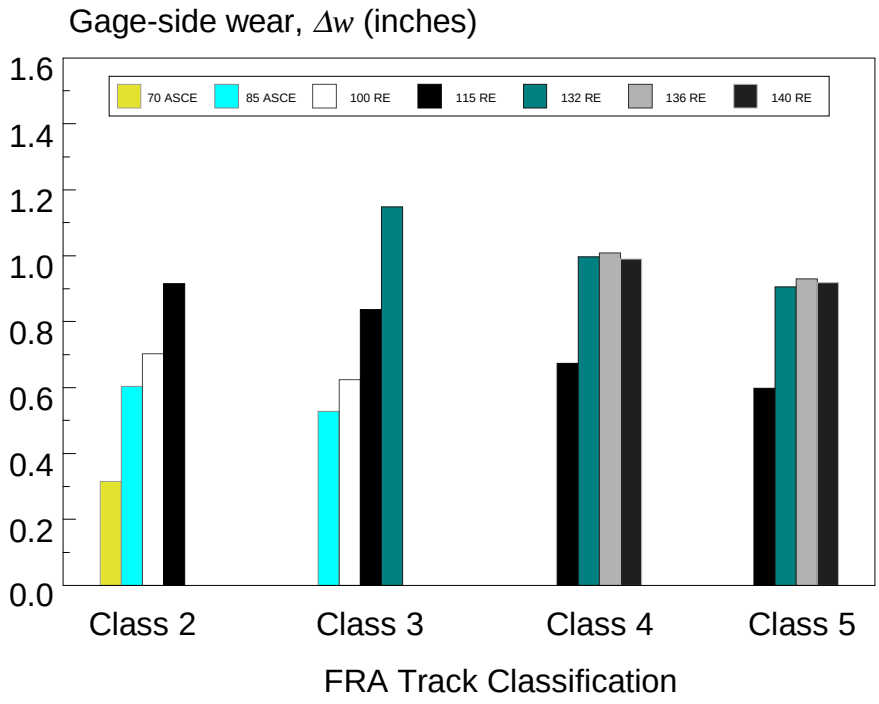

Figure 18. Wear-Limit Estimates for Side Wear Based on Fracture Strength

6. DISCUSSION AND CONCLUSIONS

Wear limits were estimated on the basis of two strength criteria: one considers failure as permanent plastic yielding, and the other considers failure when the rail fractures. The analyses that consider rail fracture assumed the presence of an internal defect (known as the detail fracture).

Worst-case wheel loads were estimated using actual freight car load data from the Northeast Corridor that were correlated with the AREA formula for dynamic load magnification. Regression analyses were conducted to extrapolate worst case dynamic wheel loads for operating conditions other than those on the Northeast Corridor. The worst case wheel loads for permanent rail bending are expected to occur once in every 10^5 to 10^6 wheel passages. If a Gaussian distribution is assumed for the dynamic load increment, the worst case load corresponds to a 5-σ event. Worst case wheel loads for the fracture mechanics analysis assumed a maximum wheel load to occur once in every train passage (or roughly once per 400 wheel passages).

Of the two cases, the fracture mechanics approach gives the more restrictive (i.e., conservative) limits. Therefore, for safe operations on railroad tracks, allowable rail-wear limits should be established on the basis of fracture strength. With the exception of the lightest rail sections considered (70 ASCE on Class 2 track and 85 ASCE on Classes 2 and 3 track), the fracture-strength-based limits can be summarized as: (1) maximum allowable head-height loss of 0.5 inch; or (2) maximum allowable gage-face wear of 0.6 inch. The basis for estimating these limits also included an assumption of a 20-MGT inspection interval, which represents typical industry practice. The same general basis would lead to larger amounts of allowable wear if more frequent inspection were assumed.

It should be noted that 70 ASCE and 85 ASCE rail sections are typically found more often in bolted joint rail (BJR) track rather than in CWR track. The most common rail defects encountered in BJR track are cracks emanating from bolt holes rather than detail fractures. In principle, it would appear that more reasonable rail wear limits for these lighter rail sizes may be estimated by modifying the fracture mechanics analysis to consider bolt hole cracks rather than detail fractures. But a potential problem in such analysis is that, to date, a validated model to determine the growth rate of bolt hole cracks has not been developed.

REFERENCES

[1] M. Hetenyi, *Beams on Elastic Foundation,* University of Michigan Press, Ann Arbor, MI, 1983.

[2] D.Y. Jeong, et al., “Propagation Analysis of Transverse Defects Originating at the Lower Gage Corner of Rail,” Final Report, DOT/FRA/ORD-98/06, 1996.

[3] P.G. Hodge, Jr., *Plastic Analysis of Structures,* McGraw-Hill, New York, NY, 1959.

[4] O. Orringer, et al., “Crack Propagation Life of Detail Fractures in Rails,” Final Report, DOT/FRA/ORD-88/13, 1988.

[5] P. Clayton and Y.H. Tang, “Detail Fracture Growth in Curved Track at the Facility for Accelerated Service Testing,” *Residual Stresses in Rails, Vol. 1,* Kluwer Academic Publishers, The Netherlands, pp. 37-56 (1992).

[6] G.M. McGee, “Calculations of Rail Bending Stresses for 125 Ton Tank Cars,” AAR Research Center Report No. 19506, Chicago, IL, April 1965.

[7] D.R. Ahlbeck, M.R. Johnson, H.D. Harrison, and J.M. Tuten, “Measurements of Wheel/Rail Loads on Class 5 Track,” Final Report, DOT/FRA/ORD-80/19, 1980.

[8] M.R. Johnson, “Summarization and Comparison of Freight Car Truck Load Data,” *ASME Transactions, Journal of Engineering for Industry 100,* 60-66 (1978).

[9] A.M. Zarembski, “Effect of Rail Section and Traffic on Rail Fatigue Life,” *American Railway Engineering Association Bulletin 673,* 514-527 (1979).

[10] J.M. Tuten and H.D. Harrison, “Design, Validation, and Application of a Monitoring Device for Measuring Dynamic Wheel/Rail Loads,” *Proceedings of the ASME Winter Annual Meeting,* Paper No. 84-WA/RT-10 (1984).

[11] R.A. Everett, Jr., F.D. Bartlett, Jr., and W. Elber, “Probabilistic Fatigue Methodology for Safe Retirement Lives,” *Journal of the American Helicopter Society,* 41-53 (1992).

APPENDIX A. SECTION PROPERTIES FOR NEW OR UNWORN RAIL

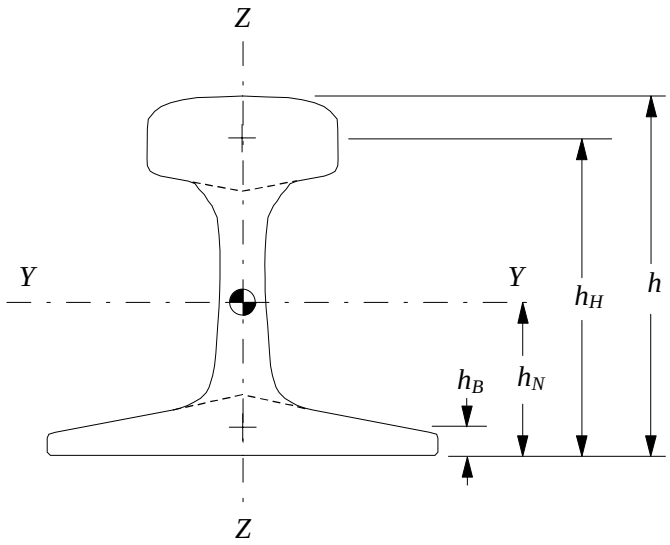

Figure A-1. Dimensions for a Generic Rail Section

NOMENCLATURE

Rail Dimensions (in)

h Total rail height
h_H Distance from the bottom of the rail to the centroid of the rail head
h_N Distance from the bottom of the rail to the centroid of the entire rail
h_B Distance from the bottom of the rail to the centroid of the rail base
w_H Rail head width

Cross-Sectional Areas (in^2)

A_R Cross-sectional area of the entire rail
A_H Cross-sectional area for the rail head only
A_W Cross-sectional area for the rail web only
A_B Cross-sectional area for the rail base only

Second Area Moments of Inertia (in^4)

I_{yy} Vertical bending inertia for the entire rail
I_{zz} Lateral bending inertia for the entire rail
I_{yyH} Vertical bending inertia for the rail head only
I_{zzH} Lateral bending inertia for the rail head only

Table A-1. Section Properties for New or Unworn Rail

	70 ASCE	***85 ASCE***	***100 RE***	***115 RE***	***132 RE***	***136 RE***	***140 RE***
h	4.625	5.188	6.00	6.625	7.125	7.313	7.313
h_H	4.01	4.46	5.23	5.80	6.3	6.39	6.35
h_N	2.22	2.47	2.75	2.98	3.2	3.35	3.37
h_B	0.299	0.321	0.394	0.411	0.436	0.435	0.436
w_H	2.4375	2.5625	2.6875	2.7188	3.00	2.9375	3.00
A_R	6.81	8.33	9.95	11.26	12.95	13.35	13.8
A_H	2.81	3.49	3.80	3.91	4.42	4.86	5.00
A_W	1.41	2.25	2.23	3.16	3.67	3.62	3.94
A_B	2.59	2.59	3.92	4.19	4.86	4.87	4.86
I_{yy}	19.7	30.07	49.0	65.6	88.1	94.9	96.8
I_{zz}	4.86	6.95	9.35	10.4	14.2	14.5	14.7
I_{yyH}	0.329	0.558	0.714	0.729	0.837	1.17	1.38
I_{zzH}	1.24	1.75	2.12	2.13	2.84	3.03	3.14

APPENDIX B. APPROXIMATION OF WORN RAIL SECTION PROPERTIES

In this report, wear is assumed to occur from uniform loss of material from the rail head. In this appendix, the amount of wear is quantified by a percentage of the rail-head area, which can be related to head-height loss or gage-face side wear. Moreover, the equations to determine the section properties that are needed in the stress analysis of worn rails are listed in this appendix. These equations were derived from idealizing the actual rail cross-section as three rectangular sections representing the head, web, and base of the rail. The specific details in deriving the equations for vertical head-height loss and gage-face side wear can be found in Jeong, et al., [2].

Equivalence between the actual and idealized rails is achieved by matching section properties for both cross-sections. In particular, the second area moments of inertia for the rail-head about the vertical and horizontal axes through the centroids for the actual and idealized rail-heads are related by

$$I_{yyH} = \frac{1}{12} \cdot h_{eq}^3 \cdot w_{eq} \qquad\qquad I_{zzH} = \frac{1}{12} \cdot h_{eq} \cdot w_{eq}^3 \tag{B-1}$$

where h_{eq} and w_{eq} are the equivalent rail-head height and width. After some algebraic manipulations, expressions for the equivalent rail-head height and width can be found

$$h_{eq} = \sqrt[8]{144 \frac{I_{yyH}^3}{I_{zzH}}} \qquad\qquad w_{eq} = \sqrt[8]{144 \frac{I_{zzH}^3}{I_{yyH}}} \,. \tag{B-2}$$

Numerical values of the equivalent rail-head heights and widths for the rail sections examined in this report, as determined from equations (B-2), are listed in Table B-1. The table also shows the magnitude of the rail-head cross-sectional area approximated by the product of these equivalent dimensions, and the percentage difference between the approximate area and the actual rail-head area.

Table B-1. Equivalent Rail-Head Height and Width for Various Rail Sections

	70 ASCE	***85 ASCE***	***100 RE***	***115 RE***	***132 RE***	***136 RE***	***140 RE***
h_{eq}	1.19	1.39	1.49	1.50	1.53	1.72	1.82
w_{eq}	2.32	2.47	2.57	2.57	2.82	2.77	2.74
$h_{eq} \times w_{eq}$	2.77	3.44	3.84	3.87	4.30	4.75	4.99
A_H	2.81	3.49	3.80	3.91	4.42	4.86	5.00
% diff. in A_H	-1.5%	-1.4%	+1.1%	-1.1%	-2.6%	-2.2%	-0.2%

The section properties for worn rail are calculated with the aid of these equivalent dimensions and by assuming a wear pattern; i.e., head-height loss or gage-face side wear.

Head-Height Loss

The following equations are applied to determine section properties for rail affected by wear in terms of head-height loss. The loss of rail-head height and the equivalent rail-head height are related by

$$\Delta h = \left(\frac{X}{100} \right) \cdot h_{eq} \tag{B-3}$$

where X is the percentage of worn rail-head area. The second area moment of inertia for vertical bending for a worn rail is calculated from

$$I_{yy}(X) = I_{Y'Y'} + A_R \cdot \left[h_N(0) - h_N(X) \right]^2 - \frac{1}{12} \cdot \Delta h^3 \cdot w_{eq} \ldots$$
$$- \left[\Delta h \cdot w_{eq} \right] \cdot \left[h - \frac{1}{2} \cdot \Delta h - h_N(X) \right]^2 . \tag{B-4}$$

In this notation, $I_{Y'Y'}$ is the vertical bending inertia of the new or unworn rail, $h_N(0)$ refers to the distance from the bottom of the rail to the centroid of the new or unworn rail, and $h_N(X)$ is the distance from the bottom of the rail to the centroid of the worn rail, which is calculated from

$$h_N(X) = \frac{A_R \cdot h_N(0) - A_H \cdot h_H(0) + \left[\left(1 - \frac{X}{100} \right) \cdot A_H \right] \cdot h_H(X)}{A_B + A_W + \left[\left(1 - \frac{X}{100} \right) \cdot A_H \right]} . \tag{B-5}$$

where A_R is the cross-sectional area of the unworn rail. The distance from the bottom of the rail to the centroid for the rail head only in a worn rail is calculated from

$$h_H(X) = h - \frac{1}{2} \cdot \Delta h . \tag{B-6}$$

where h is the total height of the rail.

Gage-Face Side Wear

The following equations are used to calculate section properties for rail affected by gage-face side wear. The amount of gage-face side wear is related to the equivalent head width by

$$\Delta w = \left(\frac{X}{100} \right) \cdot w_{eq} \ . \tag{B-7}$$

The second area moments of inertia for vertical and lateral bending of a worn rail, in this case, are calculated, respectively, from

$$I_{yy}(X) = I_{Y'Y'} + A_R \cdot \left[h_N(0) - h_N(X) \right]^2 - \frac{1}{12} \cdot {h_{eq}}^3 \cdot \Delta w \cdots$$
$$- \left[h_{eq} \cdot \Delta w \right] \cdot \left[h - \frac{1}{2} \cdot h_{eq} - h_N(X) \right]^2 \tag{B-8}$$

$$I_{zz}(X) = I_{Z'Z'} + A_R \cdot y_N(X)^2 - \frac{h_{eq}}{12} \cdot \Delta w^3 \cdots$$
$$- \left[h_{eq} \cdot \Delta w \right] \cdot \left[\frac{1}{2} \cdot \left(w_{eq} - \Delta w \right) - y_N(X) \right]^2 \tag{B-9}$$

A consequence of gage-face side wear is that the rail cross-section is asymmetric with respect to the mid-plane centerline of the rail. Further, the coordinates of the centroid for the entire rail and for the rail head only are not located on the mid-plane centerline, as they are for a new or unworn rail (Figure B-1).

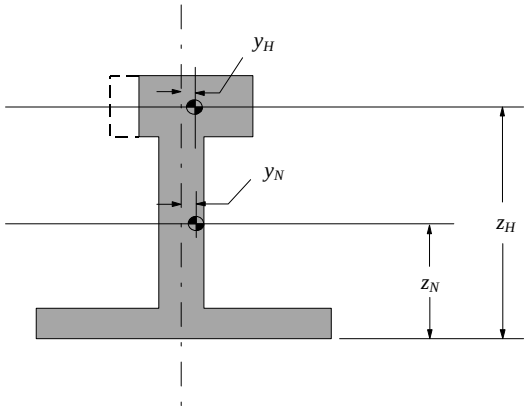

Figure B-1. Location of Centroids in Rail with Gage-Face Side Wear

The location of the centroid for the entire worn rail is defined by

$$y_N(X) = \frac{\left[\left(1 - \frac{X}{100}\right) \cdot A_H\right] \cdot y_H(X)}{A_B + A_W + \left[\left(1 - \frac{X}{100}\right) \cdot A_H\right]} \tag{B-10}$$

$$h_N(X) = \frac{A_R \cdot h_N(0) - A_H \cdot h_H(0) \cdot \left(\frac{X}{100}\right)}{A_B + A_W + \left[\left(1 - \frac{X}{100}\right) \cdot A_H\right]}. \tag{B-11}$$

The vertical location for the centroid of the worn rail head only is assumed to remain unchanged from that of the new or unworn rail head. The horizontal location of the centroid for the worn rail head only is calculated by

$$y_H(X) = \frac{1}{2} \cdot \Delta w \tag{B-12}$$

APPENDIX C. STRESS-GRADIENT MAGNIFICATION FACTOR FOR FRACTURE ANALYSIS

The handbook formulas for the stress intensity factor associated with an elliptical flaw of aspect ratio *b/a* in a combined bending field with flaw center location (*y, z*)[6] can be expressed as

$$K_I(\theta) = \frac{2}{\pi}\sigma\sqrt{\pi a}\,M(\theta) \tag{C-1}$$

where σ is the far field stress, and $M(\theta)$ is a function of angle around the crack. This function for an elliptical flaw in the rail head is given in Hodge, J., [3] as

$$M(\theta) = \frac{M_v(\theta) + \frac{y}{z}\cdot\frac{\lambda_V}{\lambda_L}\cdot\frac{I_{yy}}{I_{zz}}\cdot\frac{L}{V}\cdot M_L(\theta)}{1 + \frac{y}{z}\cdot\frac{\lambda_V}{\lambda_L}\cdot\frac{I_{yy}}{I_{zz}}\cdot\frac{L}{V}} \tag{C-2}$$

where $1/\lambda_V$ and $1/\lambda_L$ are the characteristic vertical and lateral bending wavelengths for the rail on a given foundation, which are defined in equations (4) and (7), respectively. Also, I_{yy} and I_{zz} are the second area moments of the rail section for vertical and lateral bending, L/V is the ratio of lateral to vertical load, and

$$M_v(\theta) = 1 + \frac{(b/z)\kappa^2 E_I(\kappa)\sin\theta}{(1+\kappa^2)E_I(\kappa) + (1-\kappa^2)E_{II}(\kappa)} \tag{C-3}$$

and

$$M_L(\theta) = 1 + \frac{(a/y)\kappa^2 E_I(\kappa)\cos\theta}{(1-2\kappa^2)E_I(\kappa) - (1-\kappa^2)E_{II}(\kappa)} \tag{C-4}$$

where $\kappa^2 = 1-(b/a)^2$. In equations (C-3) and (C-4), E_I and E_{II} are the complete elliptic integrals of the first and second kind, respectively, which are defined by

$$E_I(\kappa) = \int_0^{\pi/2}\sqrt{1-\kappa^2\sin^2\phi}\,d\phi \qquad E_{II}(\kappa) = \int_0^{\pi/2}\frac{d\phi}{\sqrt{1-\kappa^2\sin^2\phi}} \tag{C-5}$$

[6] In this formulation, the coordinates (*y, z*) refer to the location of the stress point relative to the centroidal axes of the rail section.

The dependence of the stress intensity factor on position along the crack front can be eliminated by calculating a simple average value. This concept was generalized in the crack-growth analyses of detail fractures [3] to calculate the $P^{\underline{th}}$ root-mean value where P is the exponent in the crack-growth rate equation. The stress-gradient or non-uniform stress magnification factor is defined mathematically as

$$M_G = \left[\frac{\int_0^{2\pi} M(\theta)^P \rho \, d\theta}{\int_0^{2\pi} \rho \, d\theta} \right]^{\frac{1}{P}} \tag{C-6}$$

where

$$\rho = \frac{b}{\sqrt{\sin^2 \theta + (b/a)\cos^2 \theta}} \tag{C-7}$$

is the radius to the perimeter of the ellipse. Equation (C-6) includes the special case of P = 1, which is the calculation for a simple average. In the crack-growth analyses presented in Orringer, et al., [4] and in the present analyses, P is assumed to be equal to 4.

The influence of wear on the stress-gradient magnification factor is affected through equation (C-2). Particularly, the second area moments of inertia and the characteristic wavelengths depend on the level of wear. Therefore, the stress gradient magnification factor depends not only on the level or amount of wear but also on the type of wear (i.e., vertical head-height loss or gage-side wear).

Table C-1 summarizes the stress-gradient magnification factors for 132 RE rail with various levels of vertical head-height loss. The magnification factor also varies depending on the lateral-to-vertical load ratio and sizes of the detail fracture. Similarly, Table C-2 lists the stress-gradient magnification factors for 132 RE rail with gage-face side wear.

Table C-1. Stress-Gradient Magnification Factors for 132 RE Rail Section and Vertical Head-Height Loss

(a) DF Size = 10% HA

Worn Area	***Lateral-to-Vertical Load Ratio, L/V***					
(%HA)	***0.05***	***0.10***	***0.20***	***0.30***	***0.40***	***0.50***
0	1.001	1.001	1.004	1.007	1.011	1.014
20	1.001	1.001	1.004	1.006	1.010	1.013
40	1.001	1.001	1.003	1.006	1.008	1.011
60	1.001	1.001	1.002	1.005	1.007	1.009
80	1.001	1.001	1.002	1.003	1.005	1.007

(b) DF Size = 15% HA

Worn Area	***Lateral-to-Vertical Load Ratio, L/V***					
(%HA)	***0.05***	***0.10***	***0.20***	***0.30***	***0.40***	***0.50***
0	1.001	1.002	1.007	1.012	1.018	1.023
20	1.001	1.002	1.006	1.011	1.016	1.021
40	1.001	1.002	1.005	1.009	1.014	1.018
60	1.001	1.002	1.004	1.007	1.011	1.015
80	1.001	1.001	1.003	1.005	1.008	1.011

(c) DF Size = 20% HA

Worn Area	***Lateral-to-Vertical Load Ratio, L/V***					
(%HA)	***0.05***	***0.10***	***0.20***	***0.30***	***0.40***	***0.50***
0	1.001	1.003	1.009	1.017	1.025	1.034
20	1.001	1.003	1.008	1.015	1.023	1.031
40	1.001	1.003	1.007	1.013	1.020	1.027
60	1.001	1.002	1.006	1.010	1.016	1.022
80	1.001	1.002	1.004	1.008	1.012	1.016

Table C-2. Stress-Gradient Magnification Factors for 132 RE Rail Section and Gage-Face Side Wear

(a) DF Size = 10% HA

Worn Area (%HA)	***Lateral-to-Vertical Load Ratio, L/V***					
	0.05	***0.10***	***0.20***	***0.30***	***0.40***	***0.50***
0	1.001	1.001	1.004	1.007	1.011	1.014
20	1.001	1.001	1.004	1.008	1.013	1.019
40	1.001	1.001	1.004	1.008	1.015	1.023
60	1.000	1.001	1.003	1.007	1.014	1.024
80	1.000	1.001	1.002	1.005	1.010	1.018

(b) DF Size = 15% HA

Worn Area (%HA)	***Lateral-to-Vertical Load Ratio, L/V***					
	0.05	***0.10***	***0.20***	***0.30***	***0.40***	***0.50***
0	1.001	1.002	1.007	1.012	1.018	1.023
20	1.001	1.002	1.007	1.014	1.022	1.032
40	1.001	1.002	1.006	1.014	1.025	1.039
60	1.001	1.001	1.005	1.012	1.024	1.041
80	1.000	1.001	1.003	1.008	1.016	1.031

(c) DF Size = 20% HA

Worn Area (%HA)	***Lateral-to-Vertical Load Ratio, L/V***					
	0.05	***0.10***	***0.20***	***0.30***	***0.40***	***0.50***
0	1.001	1.003	1.009	1.017	1.025	1.034
20	1.001	1.003	1.010	1.020	1.032	1.047
40	1.001	1.003	1.009	1.020	1.037	1.059
60	1.001	1.002	1.007	1.017	1.035	1.062
80	1.001	1.001	1.004	1.011	1.024	1.047